Low-3He/4He sublithospheric mantle source for the most magnesian magmas of the Karoo large igneous province

Heinonen, Jussi S.

2015-09-15

Heinonen , J S & Kurz , M D 2015 , ' Low- 3 He/ 4 He sublithospheric mantle source for the most magnesian magmas of the Karoo large igneous province ' , Earth and Planetary Science Letters , vol. 426 , pp. 305-315 . https://doi.org/10.1016/j.epsl.2015.06.030

http://hdl.handle.net/10138/156301
https://doi.org/10.1016/j.epsl.2015.06.030

acceptedVersion

Heinonen, J.S., Kurz, M.D. 2015. Low-^{3}He/^{4}He sublithospheric mantle source for the most magnesian magmas of the Karoo large igneous province. Earth and Planetary Science Letters 426, 305–315. http://dx.doi.org/10.1016/j.epsl.2015.06.030 (Author's postprint)

Low-^{3}He/^{4}He sublithospheric mantle source for the most magnesian magmas of the Karoo large igneous province

Jussi S. Heinonen [a] (PhD, corresponding author, jussi.s.heinonen@helsinki.fi, +35850-3185304)

Mark D. Kurz [b] (PhD, mkurz@whoi.edu)

[a] Finnish Museum of Natural History, P.O. Box 44, 00014 University of Helsinki, Finland
[b] Woods Hole Oceanographic Institution, 266 Woods Hole Road, MS# 25, Woods Hole, MA 02543-1050, USA

Abstract

The massive outpourings of Karoo and Ferrar continental flood basalts (CFBs) ~180 Ma ago mark the initial Jurassic rifting stages of the Gondwana supercontinent. The origin and sources of these eruptions have been debated for decades, largely due to difficulties in defining their parental melt and mantle source characteristics. Recent findings of Fe- and Mg-rich dikes (depleted ferropicrite suite) from Vestfjella, western Dronning Maud Land, Antarctica, have shed light on the composition of the deep sub-Gondwanan mantle: these magmas have been connected to upper mantle sources presently sampled by the Southwest Indian Ocean mid-ocean ridge basalts (SWIR MORBs) or to high ^{3}He/^{4}He plume-entrained non-chondritic primitive mantle sources formed early in Earth's history. In an attempt to determine their He isotopic composition and relative contributions from magmatic, cosmogenic, and radiogenic He sources, we performed in-vacuo stepwise crushing and melting analyses of olivine mineral separates, some of which were abraded to remove the outer layer of the grains. The best estimate for the mantle isotopic composition is given by a sample with the highest amount of He released (> 50%) during the first crushing step of an abraded coarse fraction. It has a ^{3}He/^{4}He of 7.03 ± 0.23 (2σ) times the atmospheric ratio (R_a), which is indistinguishable from those measured from SWIR MORBs (6.3–7.3 R_a; source ^{3}He/^{4}He ~6.4–7.6 R_a at 180 Ma) and notably lower than in the most primitive lavas from the North Atlantic Igneous Province (up to 50 R_a), considered to represent the epitome magmas from non-chondritic primitive mantle sources. Previously published trace element and isotopic (Sr, Nd, and Pb) compositions do not suggest a direct genetic link to any modern hotspot of Indian or southern Atlantic Oceans. Although influence of a mantle plume cannot be ruled out, the high magma temperatures and SWIR MORB-like geochemistry of the suite are best explained by supercontinent insulation of a precursory Indian Ocean upper mantle source. Such a model is also supported by the majority of the recent studies on the structure, geochronology, and petrology of the Karoo CFBs.

Keywords: Karoo; large igneous province; continental flood basalts; helium isotopes; mantle source

1. Introduction

The Karoo continental flood basalts (CFBs) erupted between the landmasses of modern Africa and Antarctica when they were a part of the Gondwana supercontinent ~180 Ma ago (e.g., Jourdan et al., 2005). The Karoo CFBs, and temporally and spatially related Ferrar CFBs (Fig. 1; often called the Karoo-Ferrar province), exhibit strongly lithosphere-influenced geochemical characteristics

(e.g., Hawkesworth et al., 1984; Sweeney et al., 1994; Molzahn et al., 1996; Luttinen and Furnes, 2000; Jourdan et al., 2007a; Neumann et al., 2011). This has led to difficulties in constraining their primary melt and mantle source characteristics, and, therefore, in defining their ultimate origins.

Recently, a group of rare Mg-rich dikes, the Vestfjella depleted ferropicrite suite, was described from the Vestfjella mountain range that forms an Antarctic extension of the Karoo CFB province (Fig. 2; Heinonen and Luttinen, 2008). These dikes exhibit no evidence of lithospheric sources or contamination and thus provide important information on the composition of the sublithospheric mantle during Karoo magmatism. Their generation requires that a positive thermal anomaly existed in the upper mantle during Karoo magmatism (Heinonen and Luttinen, 2010; Heinonen et al., 2015). On the basis of the major element, trace element, and isotopic (Sr, Nd, Pb, and Os) composition of the dikes, their origins have been linked to high-pressure (5–6 GPa) melting of hot asthenospheric mantle that has since cooled and is presently sampled by the modern mid-ocean ridge basalts of the Southwest Indian Ridge (SWIR MORBs; Heinonen et al., 2010), the modern successor of the Africa-Antarctica rift zone (Fig. 1). The isotopic compositions also overlap with non-chondritic primitive mantle reservoir recently suggested to be a major component in CFB plume sources (Jackson and Carlson, 2011).

Helium isotopes are a powerful indicator of ancient relatively undegassed mantle sources, having low (Th+U)/He and high $^{3}He/^{4}He$ (up to 50 times the atmospheric ratio, i.e., 50 R_a), and often referred to as primitive or primordial (e.g., Lupton and Craig, 1975; Kurz et al., 1982). Although such sources may be considered controversial in the context of whole mantle convection models, most of the models suggest a lower mantle origin (e.g., Class and Goldstein, 2005). High $^{3}He/^{4}He$ have been found in several hotspot-related rocks (e.g., Hawaii, Galapagos, and Iceland), and in the high-Mg rocks from the North Atlantic Volcanic Province (NAIP; Graham et al., 1998; Stuart et al., 2003; Starkey et al., 2009), which were used to estimate the trace element composition of a non-chondritic primitive mantle source (Jackson et al., 2010). In contrast, MORBs show relatively low $^{3}He/^{4}He$ values on average (~8 ±1 R_a; Kurz and Jenkins, 1981; Graham, 2002), with SWIR MORBs on the low end of the MORB spectrum ($^{3}He/^{4}He$ = 6.3–7.3 R_a; Georgen et al., 2003).

Helium isotopic compositions have not previously been reported for the Karoo CFBs or related rocks. This is due to the scarcity of primitive samples with fresh olivine or glass containing primary magmatic gas inclusions that would be suitable for He measurements, along with the Jurassic age of the samples. Most existing global He data are from zero age basalts, which minimizes the complexities of post-crystallization addition of nucleogenic (produced mainly by $^{6}Li(n,\alpha)^{3}H(\beta-)$ reactions), cosmogenic (from spallation near the Earth's surface), and radiogenic (generated by α-decay of U and Th) He, all of which can overprint the magmatic signature (see Kurz, 1986; Graham et al., 1998).

Here we present the first He isotopic data for rocks related to the Karoo CFBs (Vestfjella depleted ferropicrite suite). In order to estimate the effects of possible cosmogenic or radiogenic He, some of the carefully hand-picked olivine fractions were abraded (to remove the outer layer at the groundmass/phenocryst interface), step crushed in vacuum, and melted. In addition to He data, our analysis of the ultimate mantle source of the Vestfjella depleted ferropicrite suite is corroborated by detailed isotopic and trace element comparisons with relevant hotspot-related rocks.

Fig. 1. Present-day location of Karoo-Ferrar CFBs (and related dikes), Etendeka CFBs, Madagascar CFBs, Southwest Indian Ridge, and relevant oceanic plateaus, seamounts, and oceanic islands (stars) depicted. Gray diamonds indicate SWIR MORB samples that are geochemically (namely on the basis of Sr, Nd, and Pb isotopes) most similar to the depleted ferropicrite suite (AGU22-8-1, AGU22-9-2, AGU53-3-3, MELPROT-5-11-17, MELPROT-5-14-81, MELPROT-5-15-54, MELPROT-5-17-22, MELPROT-5-25-217, MELPROT-5-29-34, MELPROT-5-30-75, MELPROT-5-42-11; Hamelin and Allegre, 1985; le Roex et al., 1989; Mahoney et al., 1989, 1992; Janney et al., 2005).

2. Sample selection and analytical methods

2.1. Samples

Five ferropicritic and meimechitic dike rock samples (MgO = 17–24 wt. %; FeO^{tot} = 13–15 wt. %) representing the well-characterized ~185.5 ±1.8 Ma ($^{40}Ar/^{39}Ar$ plateau age; Luttinen et al., 2015) depleted ferropicrite suite of Vestfjella (Heinonen and Luttinen, 2008), western Dronning Maud Land, were selected for He isotopic analysis. The dikes were emplaced through a heterogeneous crust consisting of early-phase Karoo CFBs, Permian sedimentary rocks, and a crystalline basement of Archean to Phanerozoic age (Fig. 2a; see Groenewald et al., 1995). The samples were selected for the presence of fresh olivine and the field work emphasis was in obtaining unaltered, representative, samples for whole-rock geochemistry without consideration of in-situ ^{3}He production by cosmic rays. All the samples contain olivine phenocrysts that are larger than 1 mm in diameter, and exhibit very fine-grained groundmass indicative of crystallization relatively close to the surface. The coordinates and field characteristics, and detailed petrographical and geochemical descriptions of the samples are presented in Heinonen and Luttinen (2008, 2010) and Heinonen et al. (2010).

Four of the samples are from Basen nunatak that is composed dominantly of near-horizontal Karoo CFB flows and reaches the height of 580 m, about 400 m above the present ice surface (h ≈ 200 m; Fig. 2b). It exhibits a vertical ~300 m cliff on its northwestern (~distal) side and steeply dipping partially ice- and snow-covered slope on its southeastern (~proximal) side. Sample

AL/B16-98 represents an in-situ weathered dike from the exposed northeast corner of Basen (h ≈ 480 m). Dike-derived boulders AL/B1b-03, AL/B7-03, and AL/B9-03 were sampled from the coarse glacial drift deposits (h ≈ 450–470 m) in the 'backyard' of the Aboa and Wasa research stations close to the edge of the glacier on the southwestern slope of the nunatak (Fig. 2b). The boulder sampled by AL/B1b-03 exhibits chilled margin against sandstone that is likely to represent Permian sedimentary rock formations underlying the Vestfjella CFBs. It indicates that the boulders have been glacially transported on top of the nunatak from the valleys that surround it.

Sample AL/WM1e-98 was collected from an in-situ weathered dike (h ≈ 600 m) at West-Muren, a ridge-like nunatak, composed of Karoo CFBs and related intrusive rocks and exposed ~100 km southwest from Basen (Fig. 2c). The nunatak stands out only few meters above the ice surface (h ≈ 600 m) on its northwestern (~proximal) side whereas its southeastern (~distal) side dips steeply towards the ice surface on the bottom of the 'Muren valley' (h ≈ 500 m).

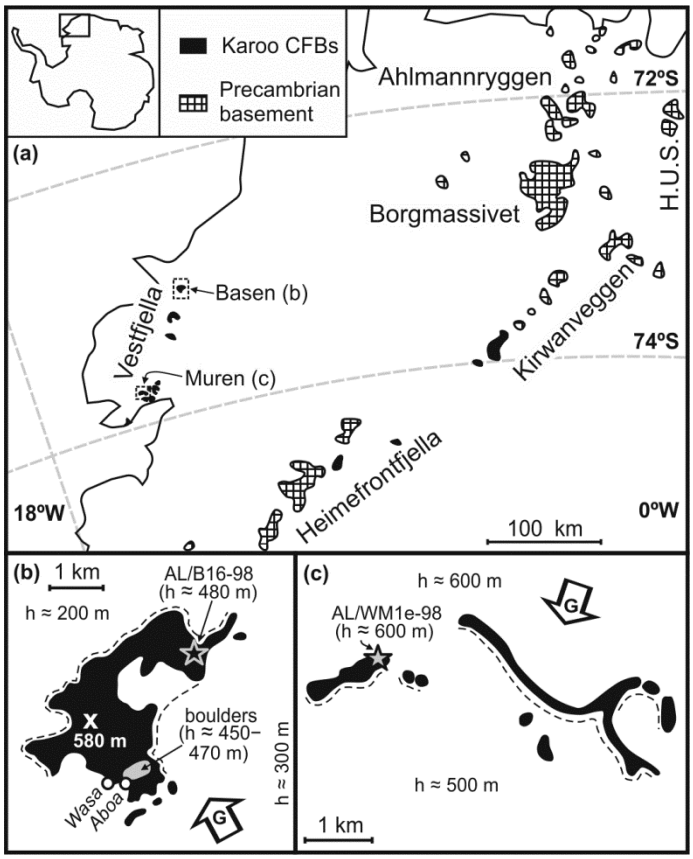

Fig. 2. Distribution of Jurassic CFBs in western Dronning Maud Land (a) and depleted ferropicrite suite sampling sites relevant to this study (b, c) shown. Location of Aboa (Finnish) and Wasa (Swedish) research stations shown in (b). Arrow marked with "G" indicates the approximate primary ice flow direction and stippled lines indicate steep cliffs in (b) and (c). H.U.S. = H. U. Sverdrupfjella.

2.2. Analytical methods

The samples were crushed multiple times with jaw crusher and several size fractions were separated from the crushed bulk sample with sieves. Although the largest olivine phenocrysts recorded on the basis of petrographical studies were over 4 mm in diameter, fractions with grain size of more than 1 mm did not contain pure olivine grains. In most samples, 0.25–0.5 mm fraction was found to be

optimum in terms of pure olivine that was still large enough for hand-picking. The relatively small grain size of pure olivine meant that at least ~1000 grains per sample had to be hand-picked to obtain enough material for abrasion and step-crushing analyses (see below). Earlier petrographical studies had revealed that many olivine grains contain large crystallized melt inclusions (Ø up to 0.8 mm) with igneous amphibole (Heinonen and Luttinen, 2010), but preliminary SEM-screenings of some of the fractions indicated that the olivines likely broke along these inclusions during crushing. The size and amount of the melt inclusions that survived the crushing are small (Ø < 0.05 mm, ~5 inclusions per 100 grains in a cross-section).

In order to estimate the effect of radiogenic ^{4}He implanted to the olivines from the surrounding groundmass after crystallization, at least one fraction from each sample was abraded to remove the outer portions of the grains. The stainless steel abrasion chamber was of the design traditionally used for zircon abrasion (Krogh, 1982), using pure nitrogen gas as the propellant. The fractions were abraded as long as needed to achieve a mass loss of 25–40% (depending on the grain size of the fraction), resulting in the removal of 20 μm thick ^{4}He-contaminated rims of the grains and uniform oval to round grain shapes (see Aciego et al., 2007). In addition to olivine fractions, one fraction consisting entirely of groundmass was separated from boulder sample AL/B9-03 (without abrasion).

The He isotopic measurements were performed at Woods Hole Oceanographic Institution (WHOI) using a dual collection and statically operated He isotope mass spectrometer that has a Nier-type ion source (locally referred to as MS2). The instrument and the procedure have been described many times in the literature, e.g., by Kurz et al. (2004). The ^{4}He blank was always below $3 \cdot 10^{-11}$ cm^{3} (STP) and small relative to the gas released from the samples. In basaltic phenocryst samples, He released by crushing in vacuum fractions is typically dominated by gas and melt inclusions (e.g., Kurz et al., 1996). The Vestfjella samples are intrusive, however, and may not have the same gas geochemistry. In most cases, the samples were crushed and analyzed in 20-stroke steps to evaluate the efficiency of gas extraction and possible post-eruption contamination (successive steps should increasingly release cosmogenic/radiogenic He from the olivine matrix). After the crushing extraction, the remaining olivine powder was melted in a single heating step and the gas analyzed to determine the bulk He isotopic composition.

3. Results and interpretation of the He isotopic measurements

3.1. Results

The results of the He measurements are shown in Table 1 and illustrated in Fig. 3. The released He contents vary from 0.001 to 0.2 μcc/g (STP) by crushing and from 0.02 to 19 μcc/g (STP) by melting: the highest amount of He was released from sample AL/WM1e-98 and from the AL/B9-03 groundmass sample having radiogenic isotopic signatures (^{3}He/^{4}He < 2 R_a). In the stepwise crushing measurements, the amount of He decreased with every step, except in the case of AL/WM1e-98 and the abraded fractions of AL/B16-98 and AL/B7-03, in all of which the second step exhibited lower He concentrations than the third (last) step. The fraction of total He released by crushing is generally below 40 %, except in the first crushing step of abraded 0.5–1 mm fraction of AL/B1b-03 (51 % of total He released). The relatively low He amount released by crushing may be the result of the rarity of melt inclusions in the olivine fractions (see section 2.2). The total He

released by melting of the AL/B9-03 groundmass fraction (4.8 μcc/g (STP)) is within the range of radiogenic ^{4}He production values (3.8–6.4 μcc/g (STP)) calculated for an age of 180 Ma and using whole-rock U (0.10 ppm) and Th (0.32 ppm) with and without subtraction of ~40 wt.% of olivine phenocrysts (as suggested by the mineral mode of the sample; Heinonen and Luttinen, 2010) having 0 ppm of U and Th.

The measured ^{3}He/^{4}He varies from 0.14 (±0.01, 2σ) R_a to 7.03 (±0.23) R_a by crushing and from 0.04 (±0.01) R_a to 15.38 (±0.47) R_a by melting. The first crushing step of abraded 0.5–1 mm fraction of AL/B1b-03 exhibits the highest crush value of 7.03 (±0.23) R_a. In the stepwise measurements, the samples that showed anomalous release of He (AL/WM1e-98 and abraded AL/B16-98 and AL/B7-03) also yielded the highest ^{3}He/^{4}He in the second step. Apart from the abraded 0.25–1 mm fraction of AL/B1b-03 that was crushed in five steps, the rest of the stepwise measurements gave the highest ^{3}He/^{4}He in the first step, although in the case of AL/B16-98 all crush ^{3}He/^{4}He values are within error.

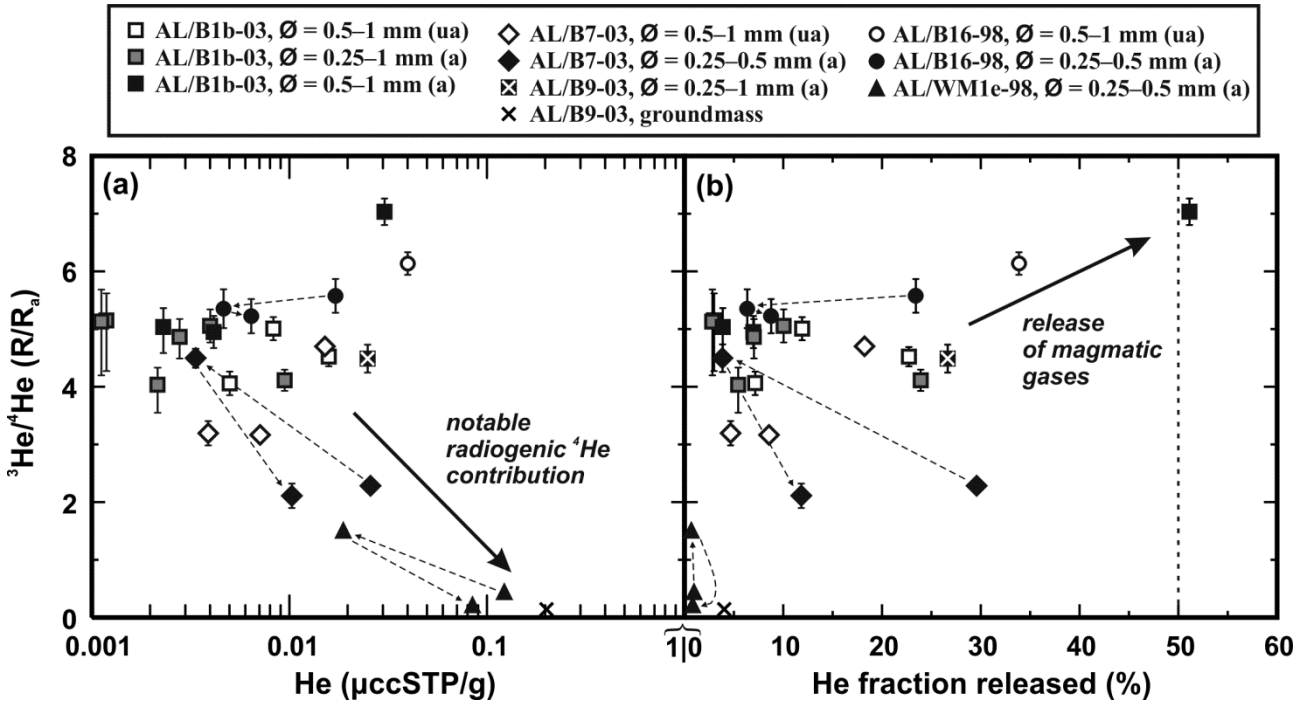

Fig. 3. Helium content and isotopic composition released by crushing of the depleted ferropicrite suite olivine fractions shown in ^{3}He/^{4}He (R/R_a) vs. He (μccSTP/g) (a) and ^{3}He/^{4}He (R/R_a) vs. He fraction released (%) (b). He fraction has been calculated for total He released, including the melt analysis. 2σ analytical error or maximum effect of nucleogenic ^{3}He production as the negative error of relevant analyses (Table 1) shown for ^{3}He/^{4}He (if larger than symbol size). Successive step crushing analyses of each sample fraction show decrease in He contents (i.e. proceed from right to left in the diagrams), except in the case of abraded AL/B7-03, AL/B16-98, and AL/WM1e-98 fractions, for which the light dashed lines connect results from step crushing for clarity (Table 1). Note that in the case of AL/B9-03 fractions and unabraded AL/B16-98 fraction, there are only data available for a single crush analysis (Table 1). The dark arrows illustrate interpretation of magmatic and radiogenic components in the olivine mineral separates. a = abraded fraction, ua = unabraded fraction.

Heinonen, J.S., Kurz, M.D. 2015. Low-^{3}He/^{4}He sublithospheric mantle source for the most magnesian magmas of the Karoo large igneous province. Earth and Planetary Science Letters 426, 305–315. http://dx.doi.org/10.1016/j.epsl.2015.06.030 (Author's postprint)

Table 1 Helium isotopic composition of the Vestfjella depleted ferropicrite suite

Sample	features*	olivine Ø [mm]	weight [g]	step	^{4}He [µccSTP/g]	^{4}He [%]	^{3}He/^{4}He (R/R_a)	2σ (R/R_a)	N-^{3}He err.# (R/R_a)
AL/B1b-03	boulder	0.5–1		1	0.0158	22.7	4.52	0.17	-0.07
	MgO = 19 wt.%	unabraded		2	0.0083	11.9	5.01	0.20	-0.13
	FeO^{tot} = 13 wt.%			3	0.0050	7.2	4.06	0.20	**-0.21**
	U = 0.13 ppm		0.263	$crush_{TOT}$	0.0291	41.8	4.58	0.18	-0.04
	Th = 0.43 ppm		0.251	melt	0.0405	58.2	4.23	0.14	-0.03
				TOTAL	0.0696	100	4.38	0.16	-0.01
		0.25–1		1	0.0095	23.9	4.11	0.18	-0.11
		abraded		2	0.0040	10.0	5.05	0.29	-0.26
				3	0.0028	7.0	4.86	0.31	**-0.37**
				4	0.0022	5.4	4.03	0.30	**-0.48**
				5	0.0012	3.0	5.15	0.47	**-0.88**
				6	0.0011	2.8	5.13	0.56	**-0.93**
			0.220	$crush_{TOT}$	0.0207	52.3	4.50	0.27	-0.05
			0.206	melt	0.0189	47.7	8.10	0.26	-0.06
				TOTAL	0.0395	100	6.22	0.27	-0.03
		0.5–1		1	0.0303	51.1	7.03	0.23	-0.03
		abraded		2	0.0041	7.0	4.95	0.28	-0.25
				3	0.0023	3.9	5.03	0.33	**-0.45**
			0.209	$crush_{TOT}$	0.0367	62.0	6.67	0.24	-0.03
			0.194	melt	0.0225	38.0	7.25	0.24	-0.05
				TOTAL	0.0592	100	6.89	0.24	-0.02
AL/B7-03	boulder	0.5–1		1	0.0151	18.2	4.70	0.18	-0.05
	MgO = 19 wt.%	unabraded		2	0.0071	8.6	3.16	0.16	-0.11
	FeO^{tot} = 13 wt.%			3	0.0039	4.7	3.19	0.21	-0.20
	U = 0.14 ppm		0.208	$crush_{TOT}$	0.0261	31.5	4.06	0.18	-0.03
	Th = 0.45 ppm		0.199	melt	0.0568	68.5	3.97	0.13	-0.01
				TOTAL	0.0829	100	3.99	0.15	-0.01
		0.25–0.5		1	0.0257	29.6	2.28	0.08	-0.03
		abraded		2	0.0034	3.9	4.49	0.24	-0.23
				3	0.0103	11.8	2.11	0.10	-0.07
			0.315	$crush_{TOT}$	0.0393	45.3	2.43	0.10	-0.02
			0.305	melt	0.0476	54.7	6.40	0.19	-0.02
				TOTAL	0.0869	100	4.60	0.15	-0.01
AL/B9-03	boulder	0.25–1	0.332	$crush_{TOT}$	0.0249	26.6	4.49	0.24	-0.02
	MgO = 24 wt.%	abraded	0.322	melt	0.0684	73.4	3.67	0.20	-0.01
	FeO^{tot} = 13 wt.%			TOTAL	0.0933	100	3.89	0.21	0.00
	U = 0.10 ppm	gm	0.300	$crush_{TOT}$	0.2001	4.0	0.14	0.01	0.00
	Th = 0.32 ppm	unabraded	0.289	melt	4.7690	96.0	0.11	0.01	0.00
				TOTAL	4.9691	100	0.11	0.01	0.00
AL/B16-98	dike	0.5–1	0.279	$crush_{TOT}$	0.0249	26.6	6.14	0.19	-0.02
	MgO = 17 wt.%	unabraded	0.264	melt	0.0684	73.4	10.26	0.31	-0.01
	FeO^{tot} = 15 wt.%			TOTAL	0.0933	100	8.86	0.27	-0.06
	U = 0.21 ppm	0.25–0.5		1	0.0171	23.4	5.57	0.29	-0.05
	Th = 0.86 ppm	abraded		2	0.0046	6.4	5.35	0.34	-0.20
				3	0.0064	8.8	5.22	0.30	-0.14
			0.258	$crush_{TOT}$	0.0281	38.6	5.46	0.30	-0.03
			0.245	melt	0.0449	61.4	15.38	0.47	-0.02
				TOTAL	0.0730	100	11.55	0.40	-0.01
AL/WM1e-98	dike	0.25–0.5		1	0.1223	0.6	0.44	0.03	-0.01
	MgO = 19 wt.%	abraded		2	0.0187	0.1	1.50	0.10	-0.07
	FeO^{tot} = 15 wt.%			3	0.0845	0.4	0.21	0.02	-0.02
	U = 0.15 ppm		0.153	$crush_{TOT}$	0.2255	1.2	0.44	0.03	-0.01
	Th = 0.49 ppm		0.138	melt	19.2000	98.8	0.04	0.01	0.00
				TOTAL	19.4255	100	0.04	0.01	0.00

* Whole-rock geochemical data from Heinonen and Luttinen (2008); # Maximum effect of nucleogenic ^{3}He growth on the R/R_a value calculated using the equations presented by Andrews (1985), neutron capture cross-sections provided for 17 elements presented by Andrews and Kay (1982), and whole-rock chemistry presented by Heinonen and Luttinen (2008). Li, B, Cl, and Co contents of the samples are unknown but required for the calculations, so they were estimated using the following trace element ratios: K/Li = 118.64(La/Yb) + 17.77(see Ryan and Langmuir, 1993), B/K = 0.001 (see Ryan and Langmuir, 1993), Cl/K = 0.04 (see Stronick and Haase, 2004), and Ni/Co = 6 (see Le Roux et al., 2011).

3.2. Constraining the magmatic $^{3}He/^{4}He$ composition

Determination of magmatic $^{3}He/^{4}He$ in Jurassic samples is complicated by post-crystallization addition of nucleogenic ^{3}He from $^{6}Li(n,\alpha)^{3}H(\beta-)$, cosmogenic ^{3}He (by spallation), and radiogenic ^{4}He (formed by the α-decay of U and Th) from the groundmass (e.g., Graham et al., 1998).

Nucleogenic ^{3}He addition in 180 Ma was calculated following the equations presented by Andrews (1985) and using neutron capture cross-sections provided for 17 elements presented by Andrews and Kay (1982). The neutron capture probabilities and neutron production rates were calculated using whole-rock chemistry of the samples. This treatment yields an upper limit to possible influence of nucleogenic ^{3}He, because pure olivine has considerably lower U and Th contents compared to the whole-rock values and thus likely smaller α-particle flux for inducing the Li reaction. The calculated effect of nucleogenic ^{3}He production is generally very small, but in the few cases in which ^{3}He contents are low (third and further crushing steps of AL/B1b-03 fractions), the net effect of estimated maximum nucleogenic ^{3}He production exceeds the 2σ error of the $^{3}He/^{4}He$ value (Table 1). In these analyses it is presented as a negative uncertainty (Table 1; Fig. 3), even though nucleogenic ^{3}He is likely to be released mainly during melting of the crushed powder.

The effect of cosmogenic ^{3}He addition is difficult to estimate, because all of the sampling sites have experienced at least some exposure to cosmic rays and exposure age constraints are lacking. Although the radiocarbon ages of snow petrel nesting sites at Vestfjella do not exceed 9000 BP (Lintinen and Nenonen, 1997), preliminary ^{10}Be age data indicates that at least some of the outcrops may have been exposed for tens of thousands of years (P. Lintinen, personal communication), and it is not possible to exclude multiple exposures produced by glacial advance and retreat. Highest melt $^{3}He/^{4}He$ (10–15 R_a) is shown by AL/B16-98 fractions (Table 1), collected from an in-situ weathered dike on Basen nunatak: their $^{3}He/^{4}He$ has likely been affected by at least some cosmogenic ^{3}He addition. Assuming initial $^{3}He/^{4}He$ of 7 R_a (see below) and no radiogenic input of ^{4}He, and using the mean global sea level high latitude cosmogenic ^{3}He production rate of 120 atoms g^{-1} yr^{-1} (Goehring et al., 2010) and scaling factor of 1.25 for Antarctica (Stone, 2000), the melt R_a value of 15 R_a shown by the abraded AL/B16-98 fraction would have been produced in ~100 ka. Outcrop exposure ages of such magnitude within a few hundred meters above the present ice/bedrock contact have been reported from elsewhere in western Dronning Maud Land and East Antarctica (e.g., Liu et al., 2010). Relatively lower melt $^{3}He/^{4}He$ values (0–8 R_a) are shown by the boulders and dike sample AL/WM1e-98, all collected very close to the continental ice sheet (Fig. 2). Although we cannot rule out cosmogenic ^{3}He influence in these cases either, it has likely been less than for AL/B16-98. Importantly, AL/B16-98 shows similar crush $^{3}He/^{4}He$ values with the boulder samples (Fig. 3), indicating that possible cosmogenic ^{3}He is primarily entrained in the olivine crystal lattice and has not significantly equilibrated with the gas-bearing inclusions.

The presence of radiogenic ^{4}He in the unabraded fractions is revealed by the fact that they show lower melt $^{3}He/^{4}He$ than the abraded fractions of the same sample (Table 1; Fig. 3). The abrasion probably did not remove all of the implanted radiogenic ^{4}He, however. For example, the

very low crush and melt R_a (< 2) and high He contents of sample AL/WM1e-98 suggest strong overprinting by radiogenic ^{4}He: the groundmass in this sample is very fine-grained and average olivine grain size relatively small making the olivine fraction more vulnerable to groundmass influence and abrasion treatment less effective. This hypothesis is substantiated in Fig. 3a, in which the crushing step analyses of AL/WM1e-98 trend towards the groundmass reference sample. Relatively low crush ^{3}He/^{4}He values ($\leq$ 4 R_a) are also shown by some other fractions that include small grain sizes (Ø < 0.5 mm) or were not abraded (Table 1; Fig. 3).

The abraded coarse (Ø = 0.5–1 mm) fraction of AL/B1b-03 shows the highest total crush ^{3}He/^{4}He (6.67 R_a) and step crush ^{3}He/^{4}He (7.03 R_a; first step). It is also the only fraction that released over 50% of He during the first crushing step (Fig. 3b), indicating that the olivines contained a relatively high amount of gas-bearing inclusions. Although we cannot exclude some effect of radiogenic ^{4}He addition in this case, we interpret the value of 7.03 (±0.23) R_a, given by the first crushing step of an abraded coarse olivine fraction, as the best estimate for the magmatic ^{3}He/^{4}He of the depleted ferropicrite suite. It is very unlikely that the variably treated sample fractions all descended from ^{3}He/^{4}He values as high as shown by some of the CFB-related picrites from NAIP (~50 R_a; Stuart et al., 2003; Starkey et al., 2009) to a rather homogeneous average crush ^{3}He/^{4}He value of 4.79 R_a (σ = 1.32; excluding the strongly ^{4}He-overprinted AL/WM1e-98).

4. Geochemical comparison with basalts from SWIR and relevant hotspots

4.1. He isotopes

The closest estimate for the magmatic He isotopic composition (7.03 R_a) of the depleted ferropicrite suite is compared with the magmatic He isotopic compositions of SWIR MORB, and oceanic plateaus, seamounts, and oceanic islands of the southern Indian and Atlantic Oceans (Fig. 1) in Fig. 4.

It is important to note that the ^{3}He/^{4}He values presented for the oceanic lavas in Fig. 4 are measured values and the data has not been age-corrected for radiogenic ingrowth of ^{4}He in the mantle source. Preliminary estimates for the He isotopic evolution of SWIR MORB sources in 180 Ma can be calculated using U (0.0047 ppm), Th (0.0137 ppm), and ^{3}He (44–170 · 10^{-6} μcc/g (STP)) contents representative of depleted mantle (Salters and Stracke, 2004; Porcelli and Ballentine, 2002) and present-day ^{3}He/^{4}He of 6.3–7.3 R_a (Georgen et al., 2003). Such sources would exhibit ^{3}He/^{4}He of 6.4–7.6 R_a at 180 Ma (i.e., 0.1–0.3 R_a higher relative to present-day values), which indicates negligible effect for the age-correction at least in this case. Calculation of age-corrections for the mantle sources of oceanic islands is hampered by the lack of knowledge on U, Th, and He compositions of the different mantle components, but the above example indicates that changes of more than ~1 R_a in 180 Ma would require relatively U- and Th-enriched and/or He-depleted mantle compositions.

Many of the oceanic hotspot-derived volcanic formations exhibit relatively high present-day ^{3}He/^{4}He (>8 R_a). Values similar to the depleted ferropicrite suite (i.e. ~6–8 R_a) have been measured from SWIR MORB, Comoros Islands, Gough Island, Prince Edward Islands, Tristan da Cunha, Crozet Islands (Possession & East Islands), and Kerguelen Islands, although in the case of the latter, many samples show comparatively high ^{3}He/^{4}He (Fig. 4). The He isotopic similarity to the Prince Edward Islands is of particular interest, as the Marion hotspot presumed to feed the volcanism there

has been considered as a possible instigator of the Karoo volcanism as well (e.g., Richards et al., 1989).

Picrites from NAIP, especially the ones that have been linked to non-chondritic primitive mantle sources, show very high ^{3}He/^{4}He (up to 50 R_a; Stuart et al., 2003; Starkey et al., 2009; not shown in Fig. 4), considerably different from the magmatic value of the depleted ferropicrite suite. Unfortunately, no data exist for the Madagascar CFBs or Paraná-Etendeka CFBs, so a helium isotopic comparison is not possible.

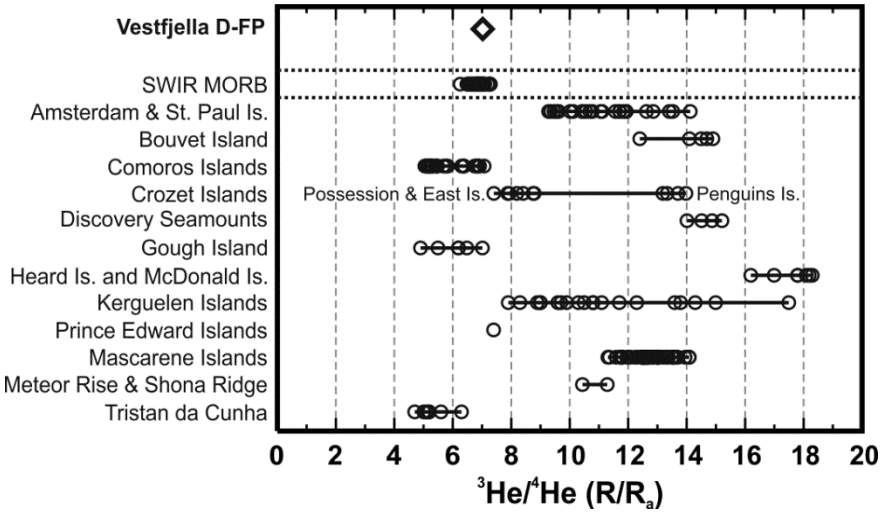

Fig. 4. Magmatic ^{3}He/^{4}He (R/R_a; the most reasonable estimate, see text) of the Vestfjella depleted ferropicrite suite, SWIR MORB, and relevant oceanic plateaus, seamounts, and oceanic islands compared (see Fig. 1). Strongly DM-influenced samples have not been included and a part of the data points represent anomalous ridge segments next to hotspots. Crozet Islands exhibit clear division into two distinct ^{3}He/^{4}He components (Possession & East Is. and Penguins Is.). Helium isotopic data for Madagascar CFBs, Etendeka CFBs, Conrad rise or Kerguelen plateau has not been published. The presented ^{3}He/^{4}He ratios are the measured ones and have not been age-corrected: the ^{3}He/^{4}He of the mantle sources is likely to change less than ~1 Ra in 180 Ma (e.g., ~0.1–0.3 R_a for the SWIR MORB source; see Section 4.1.). Data sources: Kurz et al. (1982); Hilton et al. (1995); Graham et al. (1999); Sarda et al. (2000); Hanyu et al. (2001); Georgen et al. (2003); Class et al. (2005); Doucet et al. (2006); Nicolaysen et al. (2007); Füri et al. (2011); Breton et al. (2013).

4.2. Sr, Nd, and Pb isotopes

Given the uncertainties in defining the magmatic ^{3}He/^{4}He (see section 3.2.), it is also important to consider other isotopic systems in the context of Indian Ocean and CFB magmatism. In Sr-Nd-Pb isotopic space (Figs. 5–6; all data calculated at 180 Ma; none available for Discovery Seamounts, Meteor Rise, or Shona Ridge), the great majority of the oceanic hotspots of the southern Indian and Atlantic Oceans exhibit compositions (i.e., relatively high ^{87}Sr/^{86}Sr and ^{206}Pb/^{204}Pb, and low ε_{Nd}) that indicate relative long-term enrichment in incompatible trace elements, and are distinct from those of the depleted ferropicrite suite and SWIR MORB. The depleted mantle source end-member of the Etendeka CFBs exhibits similar ^{87}Sr/^{86}Sr, ε_{Nd}, ^{206}Pb/^{204}Pb, and ^{208}Pb/^{204}Pb to the depleted ferropicrite suite, but ^{207}Pb/^{204}Pb is notably higher.

Similar age-corrected Sr, Nd, and Pb isotopic compositions with the depleted ferropicrite suite are found from NAIP, Madagascar CFBs, and SWIR MORB (Figs. 5–6). In the case of Madagascar CFBs, the high-Fe-Ti basalts and picrites having the highest ε_{Nd} and lowest ^{206}Pb/^{204}Pb (similar to

that of the depleted ferropicrite suite) have been linked to contribution from Indian Ocean upper mantle sources (those of modern SWIR MORB), whereas the compositions of the more $^{206}Pb/^{204}Pb$-enriched basalts have been linked to contribution from the Marion plume (Storey et al., 1997). In the case of SWIR MORB, the basalts that derive from sources isotopically most similar to the depleted ferropicrite suite at 180 Ma are found between 22°E and 47°E (Fig. 1). It is important to note that the SWIR MORBs that show influence of Marion hotspot (found between 36–39°E) or DUPAL isotopic signature (i.e. high $^{208}Pb/^{204}Pb$ and $^{207}Pb/^{204}Pb$ at a given $^{206}Pb/^{204}Pb$; found between 39 and 41°E) are not included in these samples (see Janney et al., 2005).

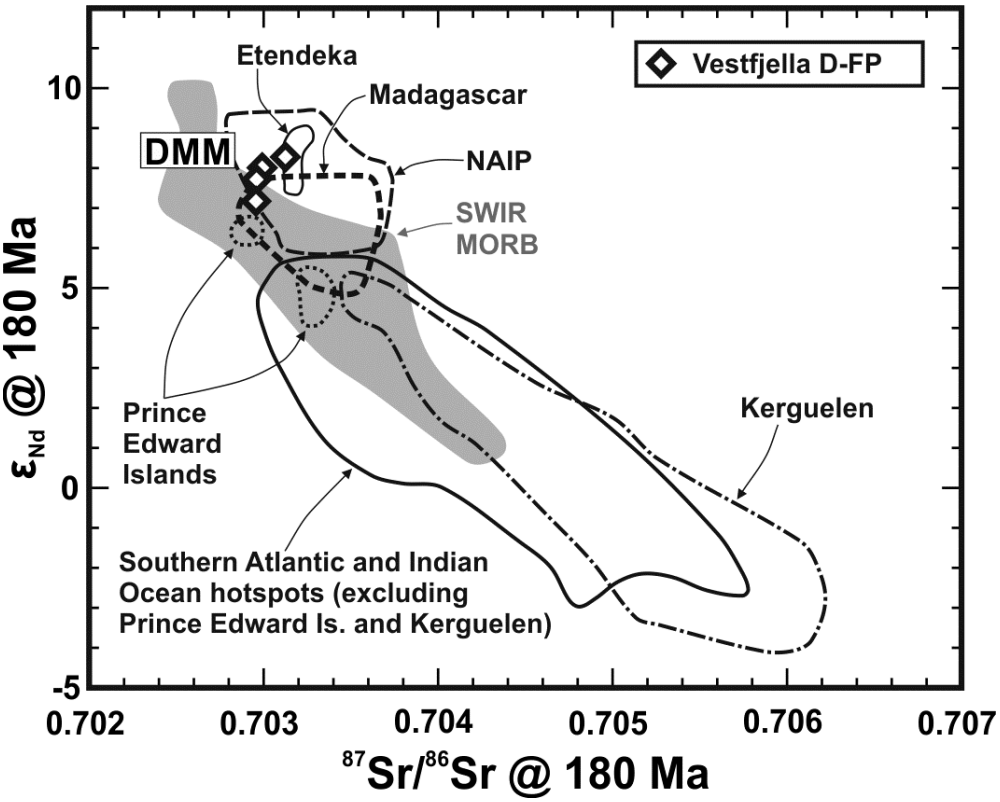

Fig. 5. Representative ε_{Nd} vs. $^{87}Sr/^{86}Sr$ compositions shown for the Vestfjella depleted ferropicrite suite and the estimated depleted sublithospheric sources of Etendeka CFBs (uncontaminated Horingbaai picrites), Madagascar CFBs (only samples with $\varepsilon_{Nd} > 5$ included), NAIP (only uncontaminated samples included), SWIR MORBs, and relevant oceanic plateaus, seamounts, and oceanic islands (see Fig. 1; Prince Edward Islands and Kerguelen hotspot-related rocks shown separately for the sake of discussion) at 180 Ma. The age-corrected source compositions for rocks younger than ~180 Ma have been estimated by first calculating the initial isotopic composition of the rocks where relevant (NAIP at 60 Ma, Madagascar at 90 Ma, Kerguelen plateau at 110 Ma, and Etendeka at 132 Ma; corrections for < 30 Ma rocks neglected) and then using $^{87}Rb/^{86}Sr$ and $^{147}Sm/^{144}Nd$ calculated on the basis of depleted MORB mantle (DMM; Workman and Hart, 2005) and bulk silicate Earth (BSE; Workman and Hart, 2005) evolution trend at the initial moment to calculate the isotopic composition of the source at 180 Ma; for example, in the case of a modern mantle-derived volcanic rock, the equations for present-day $^{87}Rb/^{86}Sr$ and $^{147}Sm/^{144}Nd$ of the source are $37.439(^{87}Sr/^{86}Sr)_i - 26.287$ and $105.25(^{143}Nd/^{144}Nd)_i - 53.759$, respectively. Continuous depletion of DMM is neglected as it does not have a significant effect in time scales relevant to this study. Data sources: Lightfoot et al. (1997); Storey et al. (1997); Graham et al. (1998); Melluso et al. (2001, 2005); Thompson et al. (2001); Stuart et al. (2003); Kent et al. (2004); Heinonen and Luttinen (2008); Starkey et al. 2009; Heinonen et al. (2010); data for SWIR MORBs compiled from PetDB (www.earthchem.org/petdb) and data for oceanic plateaus, seamounts, and oceanic islands compiled from GEOROC (www.georoc.mpch-mainz.gwdg.de).

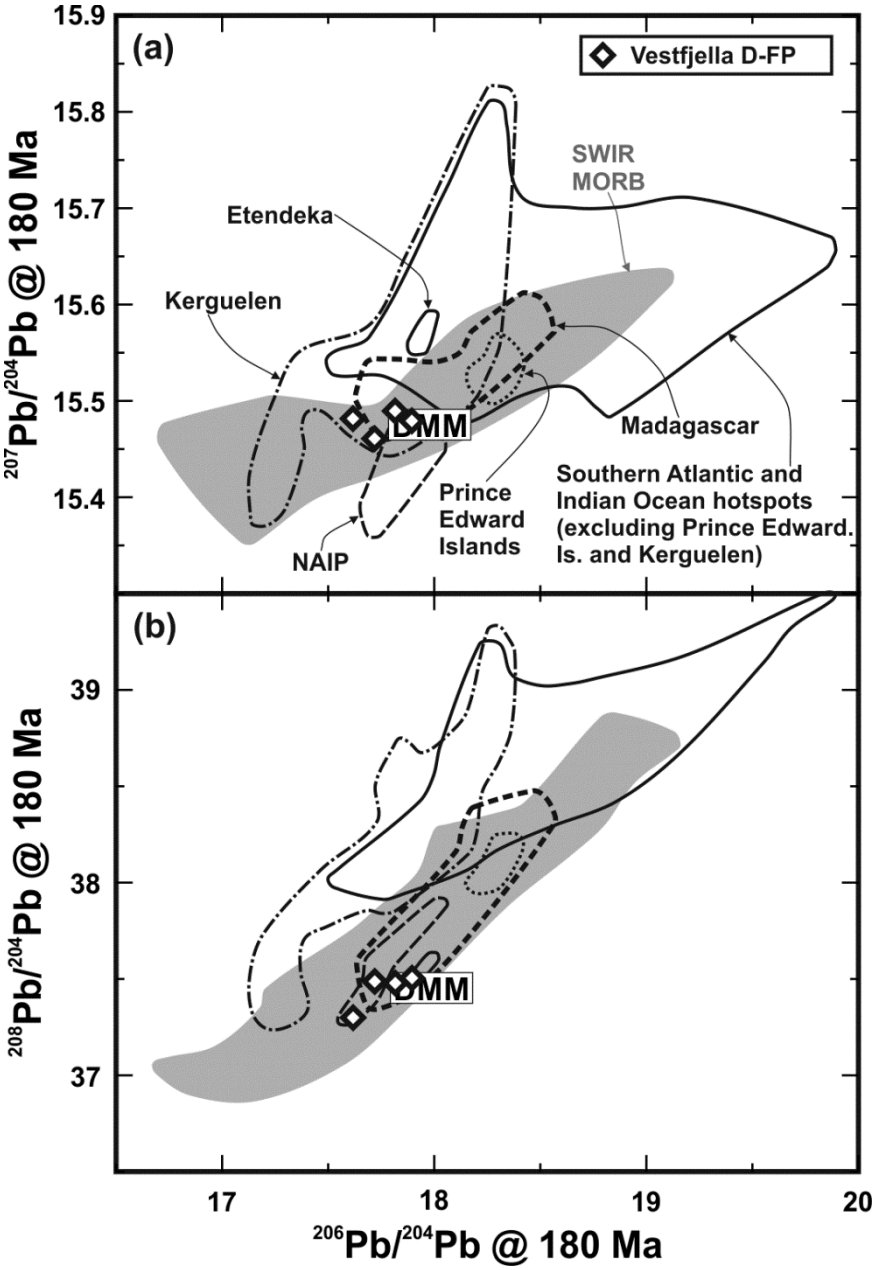

Fig. 6. Representative $^{207}Pb/^{204}Pb$ (a) and $^{208}Pb/^{204}Pb$ (b) vs. $^{206}Pb/^{204}Pb$ compositions shown for the Vestfjella depleted ferropicrite suite, Vestfjella enriched ferropicrite suite and the estimated depleted sublithospheric sources of Etendeka CFBs (uncontaminated Horingbaai picrites), Madagascar CFBs (only samples with $\varepsilon_{Nd} > 5$ included), NAIP (only uncontaminated samples included), SWIR MORBs, and relevant oceanic plateaus, seamounts, and oceanic islands (Fig. 1; Prince Edward Islands and Kerguelen hotspot-related rocks shown separately for the sake of discussion) at 180 Ma. The age-corrected source compositions for rocks younger than ~180 Ma have been estimated in a similar way as explained in Fig. 5, except that $^{238}U/^{204}Pb$ and $^{232}Th/^{204}Pb$ of the sources were calculated on the basis of age-corrected D-DMM–DMM–E-DMM trend (Workman and Hart, 2005) and by assuming present-day $(^{208}Pb/^{204}Pb)_{DMM}$ of 37.7 (Hart, 1988), $(^{208}Pb/^{204}Pb)_{D\text{-}DMM}$ of 36.9 (on the basis of correlation with global MORB $^{207}Pb/^{204}Pb$), and $(^{208}Pb/^{204}Pb)_{E\text{-}DMM}$ of 38.6 (on the basis of correlation with global MORB $^{207}Pb/^{204}Pb$). Data sources: Lightfoot et al. (1997); Storey et al. (1997); Graham et al. (1998); Thompson et al. (2001); Jourdan et al. (2007b); Heinonen et al. (2010); Jackson et al. (2010); data for SWIR MORBs compiled from PetDB (www.earthchem.org/petdb) and data for oceanic plateaus, seamounts, and oceanic islands compiled from GEOROC (www.georoc.mpch-mainz.gwdg.de).

4.3. Trace elements

Direct comparison of trace element characteristics of the depleted ferropicrite suite with SWIR MORBs and relevant CFBs and oceanic hotspots is hampered by the effects of possible secondary alteration and, notably, variable degrees and pressures of mantle melting. The Nb/Y vs. Zr/Y diagram (Fig. 7) introduced by Fitton et al. (1997), however, is not susceptible to discrepancies imposed by these processes. Firstly, Nb, Zr, and Y are high-field strength elements that are not easily mobilized by secondary processes. Secondly, although Nb/Y and Zr/Y show positive correlation with increasing pressure and decreasing degree of melting, Nb/Y *at a given* Zr/Y should not vary, unless the mantle source contained variable amounts of relatively Nb-enriched or -depleted materials (Fitton et al., 1997).

Nb/Y vs. Zr/Y diagram has been found to be highly effective in distinguishing Nb-enriched plume-sources from Nb-depleted MORB sources in Iceland (Fitton et al., 1997, 2003). In global comparison, the great majority of OIBs, E-MORBs, and anomalous ridge segments, regardless of whether they are related to thermochemical plumes or not, exhibit $\Delta Nb > 0$ [$\Delta Nb = 1.74 + \log(Nb/Y) - 1.92\log(Zr/Y)$; Fitton et al., 1997; see Fig. 7], whereas virtually all N-MORBs exhibit $\Delta Nb < 0$ (Fitton, 2007; see Fig. 7).

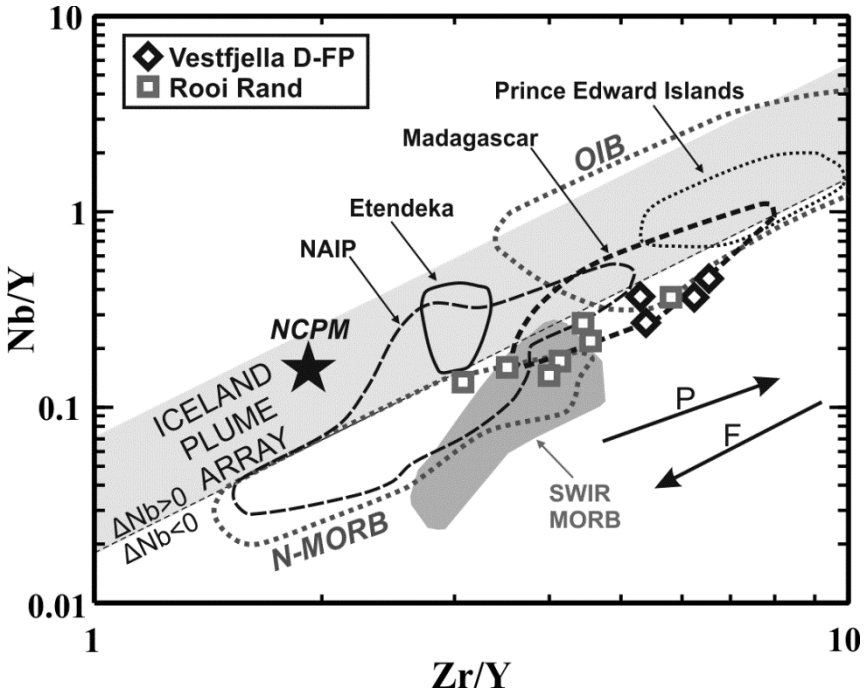

Fig. 7. Nb/Y vs. Zr/Y diagram of the Vestfjella depleted ferropicrite suite, Rooi Rand dikes of Karoo, primitive Etendeka CFBs (uncontaminated Horingbaai picrites), primitive Madagascar CFBs (only samples with $\varepsilon_{Nd} > 5$ included), primitive NAIP picrites (only samples with $\varepsilon_{Nd} > 5$ included), Marion hotspot basalts, and normal SWIR MORBs (see Figs. 5 and 6). The Iceland Plume Array and fields for N-MORB and OIB are after Fitton et al. (2003). NCPM marks the non-chondritic primitive mantle source suggested for the NAIP picrites that exhibit the highest ^{3}He/^{4}He (Jackson and Jellinek, 2013). P and F arrows denote the approximate effects of increasing pressure and degree of melting, respectively (Fitton et al., 1997). Lithospheric mantle contamination could change Nb/Y at a given Zr/Y (see Heinonen et al., 2010) so it is important to use this diagram only for uncontaminated CFB samples. Data sources: Armstrong et al. (1984); Lightfoot et al. (1997); Storey et al. (1997); Melluso et al. (2001, 2005); Thompson et al. (2001); Stuart et al. (2003); Kent et al. (2004); Starkey et al. (2009); data for SWIR MORBs compiled from PetDB (www.earthchem.org/petdb) and data for Prince Edward Islands compiled from GEOROC (www.georoc.mpch-mainz.gwdg.de).

The uncontaminated depleted ferropicrite suite samples all have $\Delta Nb < 0$ and indicate that their sources were not Nb-enriched (Fig. 7). In fact, their Nb-Zr-Y systematics can be explained by high-pressure (+low-degree?) melting of MORB-like sources and they are connected to the field of N-MORBs and SWIR MORBs by the Rooi Rand dikes of southern Lebombo that mark the first phases of oceanization of the Africa-Antarctica rift (Jourdan et al., 2007b; Fig. 7; see also Heinonen et al., 2010).

In contrast to the depleted ferropicrite suite, the CFB-related primitive samples from NAIP, Etendeka, and Madagascar are composed of or include samples with $\Delta Nb > 0$. In the case of NAIP, complex mixing of Nb-enriched sources with Nb-depleted sources is indicated by the trace element and isotopic data (Stuart et al., 2003). The estimated trace element composition of the non-chondritic primitive mantle source (Jackson and Jellinek, 2013), proposed as the main component for the most $^{3}He/^{4}He$-enriched NAIP picrites (Jackson and Carlson, 2011), exhibits high ΔNb, and thus cannot represent a viable source for the depleted ferropicrite suite. The Nb-Zr-Y composition of Madagascar CFBs indicate mixing with MORB and Marion hotspot sources, compatible with what has been suggested for them on the basis of isotopic data (Storey et al., 1997).

5. Implications for the Karoo CFBs and Indian Ocean magmatism

The depleted ferropicrite suite exhibits considerable similarity to SWIR MORBs in terms of Sr, Nd, Pb, and He isotopic compositions and incompatible trace element characteristics (Figs. 4–7). Major element modeling indicates similar degrees of dominantly peridotitic mantle melting for both suites (~10% and ~10–20%, respectively; Langmuir et al., 1992; Heinonen and Luttinen, 2010) so they likely sampled mantle heterogeneity on a roughly equal scale. The presented results are thus compatible with a common mantle source for these rocks that are separated by an age of 180 Ma and were generated in distinct tectonic settings (see also Heinonen et al., 2010). In contrast, the He isotopic results and trace element systematics (Fig. 7) preclude significant contributions from non-chondritic primitive mantle sources, and Sr, Nd, and Pb isotopic data preclude significant contributions from modern hotspots that are responsible for the generation of oceanic islands and plateaus in the Indian and southern Atlantic Oceans (Figs. 5 and 6).

One notable feature that is not directly compatible with the SWIR MORB sources for the depleted ferropicrite suite are the high crystallization temperatures (> 1600 °C; Heinonen and Luttinen, 2010) calculated on the basis of olivine-melt equilibria (method of Putirka et al., 2007). The calculations imply generation from a source that was heated more than 200 °C above ambient (and modern Indian Ocean) upper mantle temperature, despite the presence of igneous amphibole that indicates magmatic water contents of 1–2 wt. % for the parental melts (Heinonen and Luttinen, 2010). Recent study using thermometry that relies on exchange of Al between co-crystallizing olivine and spinel, and is largely independent of pressure or melt composition, suggests that estimations on the basis of olivine-liquid equilibria overshoot the actual crystallization (and possibly also mantle source) temperatures by more than 100 °C, however (Heinonen et al., 2015). In any case, the mantle potential temperature required for the generation of the high-Mg depleted ferropicrite suite is likely to be at least ~100 °C above that of ambient upper mantle.

If a mantle plume is invoked as the cause for the elevated temperatures, two different scenarios could hypothetically explain the compositional similarity of the depleted ferropicrite suite to SWIR MORB: 1) plume contains material with MORB source signature or 2) upper mantle

material was entrained into a rising plume (see Kerr et al., 1995). Scenario 1 would be the first known Phanerozoic plume of such composition as modern plume-related rocks, even if having MORB-like high ε_{Nd}, show either high ΔNb, high $^{3}He/^{4}He$, and/or anomalous Pb isotopic compositions (e.g., Hawaii, Iceland; Kerr et al., 1995; Fitton, 2007; Figs. 6 and 7). Scenario 2 is hampered by the lack of evidence on even more magnesian and hot and/or isotopically distinct sublithospheric Karoo magmas that would have been expected to form within the plume itself (see Kerr et al., 1995). On the other hand, it is important to note that the great majority of the Karoo CFBs have been contaminated by or derive from the Gondwanan lithosphere (e.g., Hawkesworth et al., 1984; Sweeney et al., 1994; Luttinen and Furnes, 2000; Jourdan et al., 2007a; Neumann et al., 2011): possible plume-derived geochemical signatures may thus have been overprinted beyond recognition (see Heinonen et al., 2014). Ellam et al. (1992) postulated mixing of lithospheric and plume sources on the basis of Os isotopic composition of the Mwenezi picrites in Africa, but the most recent studies on the Pb and Hf isotopic composition of these rocks led Ellam (2006) to favor predominant contribution from variably enriched lithospheric mantle instead. In addition to depleted ferropicrite suite and related Low-Nb magma type (Heinonen et al., 2010; Luttinen et al., 2015) of Vestfjella, the only Karoo magma types that are uncontaminated by the crust and are likely to derive dominantly from sublithospheric sources are the Vestfjella enriched ferropicrite suite (Heinonen and Luttinen, 2008; Heinonen et al., 2010), Group 3 dikes from Ahlmannryggen (Riley et al., 2005), and some high-ε_{Nd} E-MORB Rooi Rand dikes from Africa (Armstrong et al., 1984; Duncan et al., 1990). The emplacement of the Rooi Rand dikes post-dates the main CFB phase by ~10 Ma and is related to the onset of oceanization of the rifted margin (Jourdan et al., 2007b; see Fig. 7). The enriched ferropicrite suite and Group 3 dikes likely sampled recycled heterogeneities, but these magma types are not similar in isotopic composition with relevant modern hotspots, are not parental to Karoo CFBs, and are likely to pre-date (Group 3) and post-date (enriched ferropicrite suite) the main phase of Karoo magmatism (Riley et al., 2005; Heinonen and Luttinen, 2008; Heinonen et al., 2010, 2014). The suggested link between the modern Marion (or any other southern Indian Ocean or Atlantic) plume and Karoo CFBs is thus not currently supported by the geochemical data. Intriguingly, it could be argued that the generation of the Madagascar CFBs at ~90 Ma marks the arrival of the Marion plume head to the Indian Ocean mantle lithosphere (Storey et al., 1997).

The viability of the mantle plume hypothesis as an explanation for the generation of a specific magmatic province should not be evaluated by geochemistry alone (e.g., Farnetani and Hofmann, 2014). Several recent studies on the structure, geochronology, and petrology of the Karoo province are not readily compatible with the traditional mantle plume hypothesis (Le Gall et al., 2002, 2005; Watkeys, 2002; Jourdan et al., 2004, 2005, 2006, 2007a, 2009; Coltice et al., 2009; Hastie et al., 2014; cf. Ferraccioli et al., 2005; Curtis et al., 2008). One of the preferred alternative models for the Karoo CFBs is the "internal mantle heating" model, which suggests an increase in the upper mantle potential temperatures of up to more than 100 °C beneath an insulating supercontinent (Coltice et al., 2009). Favorable plate boundary assemblies prior to Gondwana breakup may have further enhanced the effect of subcontinental heating (see Rolf et al., 2012; Hastie et al., 2014). The implication of this study, that the hottest and most primitive sublithospheric magmas known from Karoo seem to sample Indian Ocean upper mantle, is compatible with such propositions. Supercontinent insulation could be further associated with drainage of slowly accumulated sublithospheric magma reservoir (Silver et al., 2006) and lithospheric delamination (Elkins-Tanton

and Hager, 2000) that could also explain the large-scale metasomatism observed in the Indian Ocean upper mantle (Janney et al., 2005; Hanan et al., 2013).

The NAIP may be one of the best examples of a plume-instigated CFB province (e.g., Brown and Lesher, 2014), but the role of mantle plumes in the generation of Karoo CFBs remains an open question. The hypothesis that all CFB provinces that were formed close to the margins of large low shear velocity provinces (LLSVPs) in the lower mantle are plume-generated (Burke and Torsvik, 2004) may thus be an overgeneralization. After all, all CFB provinces related to the early stages of Pangea and Gondwana breakup (i.e. Central Atlantic Magmatic Province, Ferrar, and Karoo) have been presented as the best Phanerozoic candidates for internal mantle heating models (Coltice et al., 2009; Hastie et al., 2014; Hole, 2015), and at least one of them hosts high-temperature picrites generated from a low-^{3}He/^{4}He, long-term depleted mantle source.

6. Conclusions

The age of the Karoo CFB eruptions presents challenges to obtaining the mantle helium isotopic compositions, given the presence of radiogenic and cosmogenic helium. The analytical strategy utilized here, of abrasion and coupled crushing/melting in vacuum, shows that it is possible to estimate the effects of different helium components to the total ^{3}He/^{4}He in these samples. The best estimate for the magmatic ^{3}He/^{4}He isotopic composition (obtained from a fresh, abraded, and coarse olivine fraction) of the most magnesian Karoo CFB magma type (Vestfjella depleted ferropicrite suite) is 7.03 ±0.23 R_a. This value is similar to those obtained from SWIR MORBs (6.3–7.3 R_a; source ^{3}He/^{4}He ~6.4–7.6 R_a at 180 Ma) and notably lower than those measured from most of the southern Atlantic or Indian Ocean hotspots, or CFB-related high-Mg rocks thought to derive from early-formed non-chondritic primitive mantle sources. Trace element, Sr, Nd, and Pb isotopic comparisons further consolidate these relationships. The composition and high-T origin of the suite are best explained by supercontinent insulation of a precursory Indian Ocean upper mantle source, which is also preferred on the basis of the latest structural, geochronological, and petrological studies on the Karoo CFBs.

Acknowledgements

Comments by the handling editor Michael Bickle and thoughtful and honest reviews by David Graham and Godfrey Fitton encouraged us to considerably enhance the discussion from its original state. Arto Luttinen, Rick Carlson, Matt Jackson, and Takeshi Hanyu are thanked for contributing to the initial ideas and encouragement for the research. Riina Puttonen is thanked for the tremendous work she did in separating and hand-picking thousands and thousands of miniscule olivine grains from the crushed whole-rock samples. Joshua Curtice performed equally invaluable work by running the He analyses at WHOI. Hannu Huhma and Leena Järvinen are thanked for their help in providing abrasion equipment and assistance at the Geological Survey of Finland. Petri Lintinen is thanked for discussions related to outcrop exposure ages of western Dronning Maud Land. Support for the measurements at the Isotope Geochemistry Facility at WHOI has come from the U.S. National Science Foundation (Grant No. OCE-1232985 and PLR-1043485). Our research is funded by the Academy of Finland (Grant No. 252652).

References

Aciego, S.M., DePaolo, D.J., Kennedy, B.M., Lamb, M.P., Sims, K.W.W., Dietrich, W.E., 2007. Combining [^{3}He] cosmogenic dating with U–Th/He eruption ages using olivine in basalt. Earth Planet. Sci. Lett. 254, 288-302. http://dx.doi.org/10.1016/j.epsl.2006.11.039.

Andrews, J.N., 1985. The isotopic composition of radiogenic helium and its use to study groundwater movement in confined aquifers. Chem. Geol. 49, 339-351. http://dx.doi.org/10.1016/0009-2541(85)90166-4.

Andrews, J.N., Kay, R.L.F., 1982. Natural production of tritium in permeable rocks. Nature 298, 361-363. http://dx.doi.org/10.1038/298361a0

Armstrong, R.A., Bristow, J.W., Cox, K.G., 1984. The Rooi Rand dyke swarm, southern Lebombo. In: Erlank, A.J. (Ed.), Petrogenesis of the volcanic rocks of the Karoo Province. Geol. Soc. S. Africa Spec. Pub. 13, Johannesburg, South Africa, pp. 77-86.

Breton, T., Nauret, F., Pichat, S., Moine, B., Moreira, M., Rose-Koga, E.F., Auclair, D., Bosq, C., Wavrant, L., 2013. Geochemical heterogeneities within the Crozet hotspot. Earth Planet. Sci. Lett. 376, 126-136. http://dx.doi.org/10.1016/j.epsl.2013.06.020.

Brown, E.L., Lesher, C.E., 2014. North Atlantic magmatism controlled by temperature, mantle composition and buoyancy. Nature Geosci. 7, 820-824. http://dx.doi.org/10.1038/ngeo2264.

Burke, K., Torsvik, T.H., 2004. Derivation of Large Igneous Provinces of the past 200 million years from long-term heterogeneities in the deep mantle. Earth Planet. Sci. Lett. 227, 531-538. http://dx.doi.org/10.1016/j.epsl.2004.09.015.

Class, C., Goldstein, S.L., 2005. Evolution of helium isotopes in the Earth's mantle. Nature 436, 1107-1112. http://dx.doi.org/10.1038/nature03930.

Class, C., Goldstein, S.L., Stute, M., Kurz, M.D., Schlosser, P., 2005. Grand Comore Island: A well-constrained "low ^{3}He/^{4}He" mantle plume. Earth Planet. Sci. Lett. 233, 391-409. http://dx.doi.org/10.1016/j.epsl.2005.02.029.

Coltice, N., Bertrand, H., Rey, P., Jourdan, F., Phillips, B.R., Ricard, Y., 2009. Global warming of the mantle beneath continents back to the Archaean. Gondwana Res. 15, 254-266. http://dx.doi.org/10.1016/j.gr.2008.10.001.

Curtis, M.L., Riley, T.R., Owens, W.H., Leat, P.T., Duncan, R.A., 2008. The form, distribution and anisotropy of magnetic susceptibility of Jurassic dykes in H.U. Sverdrupfjella, Dronning Maud Land, Antarctica. Implications for dyke swarm emplacement. J. Struct. Geol. 30, 1429-1447, http://dx.doi.org/10.1016/j.jsg.2008.08.004.

Doucet, S., Moreira, M., Weis, D., Scoates, J.S., Giret, A., Allègre, C., 2006. Primitive neon and helium isotopic compositions of high-MgO basalts from the Kerguelen Archipelago, Indian Ocean. Earth Planet. Sci. Lett. 241, 65-79. http://dx.doi.org/10.1016/j.epsl.2005.10.025.

Duncan, A.R., Armstrong, R.A., Erlank, A.J., Marsh, J.S., Watkins, R.T., 1990. MORB-related dolerites associated with the final phases of Karoo flood basalt volcanism in Southern Africa. In: Parker, A.J., Rickwood, P.C., Tucker, D.H. (Eds.), Mafic dykes and emplacement mechanisms. Proceedings of the Second International dyke conference, Balkema, Rotterdam, pp. 119-129.

Elkins-Tanton, L.T., Hager, B.H., 2000. Melt intrusion as a trigger for lithospheric foundering and the eruption of the Siberian flood basalts. Geophys. Res. Lett. 27, 3937-3940. http://dx.doi.org/10.1029/2000GL011751.

Ellam, R.M., 2006. New constraints on the petrogenesis of the Nuanetsi picrite basalts from Pb and Hf isotope data. Earth Planet. Sci. Lett. 245, 153-161. http://dx.doi.org/10.1016/j.epsl.2006.03.004.

Ellam, R.M., Carlson, R.W., Shirey, S.B., 1992. Evidence from Re-Os isotopes for plume-lithosphere mixing in Karoo flood basalt genesis. Nature 359, 718-721. http://dx.doi.org/10.1038/359718a0.

Farnetani, C.,G., Hofmann, A.,W., 2014. Mantle Plumes. In: Gupta, H. (Ed.), Encyclopedia of Earth Sciences Series. Springer, Netherlands, pp. 857-869. http://dx.doi.org/10.1007/978-90-481-8702-7_132.

Ferraccioli, F., Jones, P.C., Curtis, M.L., Leat, P.T., 2005. Subglacial imprints of early Gondwana break-up as identified from high resolution aerogeophysical data over western Dronning Maud Land, East Antarctica. Terra Nova 17, 573-579. http://dx.doi.org/10.1111/j.1365-3121.2005.00651.x.

Fitton, J.G., 2007. The OIB paradox. Geol. In: Foulger, G.R., Jurdy, D.M. (Eds.), Plates, Plumes and Planetary Processes. Geol. Soc. Am. Spec. Pap. 430, Boulder CO, United States, pp. 387-412. http://dx.doi.org/10.1130/2007.2430(20).

Fitton, J.G., Saunders, A.D., Norry, M.J., Hardarson, B.S., Taylor, R.N., 1997. Thermal and chemical structure of the Iceland Plume. Earth Planet. Sci. Lett. 153, 197-208. http://dx.doi.org/10.1016/s0012-821x(97)00170-2.

Fitton, J.G., Saunders, A.D., Kempton, P.D., Hardarson, B.S., 2003. Does depleted mantle form an intrinsic part of the Iceland Plume? Geochem. Geophys. Geosyst. 4. http://dx.doi.org/10.1029/2002gc000424.

Füri, E., Hilton, D.R., Murton, B.J., Hémond, C., Dyment, J., Day, J.M.D., 2011. Helium isotope variations between Réunion Island and the Central Indian Ridge (17°-21°S): New evidence for ridge-hot spot interaction. J. Geophys. Res. B 116. http://dx.doi.org/10.1029/2010JB007609.

Georgen, J.E., Kurz, M.D., Dick, H.J.B., Lin, J., 2003. Low ^{3}He/^{4}He ratios in basalt glasses from the western Southwest Indian Ridge (10°-24°E). Earth Planet. Sci. Lett. 206, 509-528. http://dx.doi.org/10.1016/S0012-821X(02)01106-8.

Goehring, B.M., Kurz, M.D., Balco, G., Schaefer, J.M., Licciardi, J., Lifton, N., 2010. A reevaluation of in situ cosmogenic ^{3}He production rates. Quat. Geochronol. 5, 410-418. http://dx.doi.org/10.1016/j.quageo.2010.03.001.

Graham, D.W., 2002. Noble Gas Isotope Geochemistry of Mid-Ocean Ridge and Ocean Island Basalts: Characterization of Mantle Source Reservoirs. In: Porcelli, D., Ballentine, C.J., Wieler, R. (Eds.), Noble Gases in Geochemistry and Cosmochemistry. Rev. Mineral. Geochem. 47, Min. Soc. Am., Washington DC, United States, pp. 247-318. http://dx.doi.org/10.2138/rmg.2002.47.8.

Graham, D.W., Larsen, L.M., Hanan, B.B., Storey, M., Pedersen, A.K., Lupton, J.E., 1998. Helium isotope composition of the early Iceland mantle plume inferred from the Tertiary picrites of West Greenland. Earth Planet. Sci. Lett. 160, 241-255. http://dx.doi.org/10.1016/S0012-821X(98)00083-1.

Graham, D.W., Johnson, K.T.M., Priebe, L.D., Lupton, J.E., 1999. Hotspot–ridge interaction along the Southeast Indian Ridge near Amsterdam and St. Paul islands: helium isotope evidence. Earth Planet. Sci. Lett. 167, 297-310. http://dx.doi.org/10.1016/S0012-821X(99)00030-8.

Groenewald, P.B., Moyes, A.B., Grantham, G.H., Krynauw, J.R., 1995. East Antarctic crustal evolution: geological constraints and modelling in western Dronning Maud Land. Precambrian Res. 75, 231-250. http://dx.doi.org/10.1016/0301-9268(95)80008-6.

Hamelin, B., Allegre, C.J., 1985. Large-scale regional units in the depleted upper mantle revealed by an isotope study of the South-West Indian Ridge. Nature 315, 196-199. http://dx.doi.org/10.1038/315196a0.

Hanan, B.B., Blichert-Toft, J., Hemond, C., Sayit, K., Agranier, A., Graham, D.W., Albarède, F., 2013. Pb and Hf isotope variations along the Southeast Indian Ridge and the dynamic distribution of MORB source domains in the upper mantle. Earth Planet. Sci. Lett. 375, 196-208. http://dx.doi.org/10.1016/j.epsl.2013.05.028.

Hanyu, T., Dunai, T.J., Davies, G.R., Kaneoka, I., Nohda, S., Uto, K., 2001. Noble gas study of the Reunion hotspot: evidence for distinct less-degassed mantle sources. Earth Planet. Sci. Lett. 193, 83-98. http://dx.doi.org/10.1016/S0012-821X(01)00489-7.

Hart, S.R., 1988. Heterogeneous mantle domains: signatures, genesis and mixing chronologies. Earth Planet. Sci. Lett. 90, 273-296. http://dx.doi.org/10.1016/0012-821X(88)90131-8.

Hastie, W.W., Watkeys, M.K., Aubourg, C., 2014. Magma flow in dyke swarms of the Karoo LIP: Implications for the mantle plume hypothesis. Gondwana Res. 25, 736-755. http://dx.doi.org/10.1016/j.gr.2013.08.010.

Hawkesworth, C.J., Marsh, J.S., Duncan, A.R., Erlank, A.J., Norry, M.J., 1984. The role of continental lithosphere in the generation of the Karoo volcanic rocks: evidence from combined Nd- and Sr-isotope studies. In: Erlank, A.J. (Ed.), Petrogenesis of the volcanic rocks of the Karoo Province. Geol. Soc. S. Africa Spec. Pub. 13, Johannesburg, South Africa, pp. 341-354.

Heinonen, J.S., Luttinen, A.V., 2008. Jurassic dikes of Vestfjella, western Dronning Maud Land, Antarctica: Geochemical tracing of ferropicrite sources. Lithos 105, 347-364. http://dx.doi.org/10.1016/j.lithos.2008.05.010.

Heinonen, J.S., Luttinen, A.V., 2010. Mineral chemical evidence for extremely magnesian subalkaline melts from the Antarctic extension of the Karoo large igneous province. Miner. Petrol. 99, 201-217. http://dx.doi.org/10.1007/s00710-010-0115-9.

Heinonen, J.S., Carlson, R.W., Luttinen, A.V., 2010. Isotopic (Sr, Nd, Pb, and Os) composition of highly magnesian dikes of Vestfjella, western Dronning Maud Land, Antarctica: A key to the origins of the Jurassic Karoo large igneous province? Chem. Geol. 277, 227-244. http://dx.doi.org/10.1016/j.chemgeo.2010.08.004.

Heinonen, J.S., Carlson, R.W., Riley, T.R., Luttinen, A.V., Horan, M.F., 2014. Subduction-modified oceanic crust mixed with a depleted mantle reservoir in the sources of the Karoo continental flood basalt province. Earth Planet. Sci. Lett. 394, 229-241. http://dx.doi.org/10.1016/j.epsl.2014.03.012.

Heinonen, J.S, Jennings, E.S., Riley, T.R., 2015. Crystallisation temperatures of the most Mg-rich magmas of the Karoo LIP on the basis of Al-in-olivine thermometry. Chem. Geol. 411, 26-35. http://dx.doi.org/10.1016/j.chemgeo.2015.06.015.

Hilton, D.R., Barling, J., Wheller, G.E., 1995. Effect of shallow-level contamination on the helium isotope systematics of ocean-island lavas. Nature 373, 330-333. http://dx.doi.org/10.1038/373330a0.

Hole, M.J., 2015. The generation of continental flood basalts by decompression melting of internally heated mantle. Geology 43, 311-314. http://dx.doi.org/10.1130/g36442.1.

Jackson, M.G., Carlson, R.W., 2011. An ancient recipe for flood-basalt genesis. Nature 476, 316-319. http://dx.doi.org/10.1038/nature10326.

Jackson, M.G., Jellinek, A.M., 2013. Major and trace element composition of the high ^{3}He/^{4}He mantle: Implications for the composition of a nonchonditic Earth. Geochem. Geophys. Geosyst. 14, 2954-2976. http://dx.doi.org/10.1002/ggge.20188.

Jackson, M.G., Carlson, R.W., Kurz, M.D., Kempton, P.D., Francis, D., Blusztajn, J., 2010. Evidence for the survival of the oldest terrestrial mantle reservoir. Nature 466, 853-856. http://dx.doi.org/10.1038/nature09287.

Janney, P.E., le Roex, A.P., Carlson, R.W., 2005. Hafnium isotope and trace element constraints on the nature of mantle heterogeneity beneath the central Southwest Indian Ridge (13°E to 47°E). J. Petrol. 46, 2427-2464. http://dx.doi.org/10.1093/petrology/egi060.

Jourdan, F., Féraud, G., Bertrand, H., Kampunzu, A.B., Tshoso, G., Le Gall, B., Tiercelin, J.J., Capiez, P., 2004. The Karoo triple junction questioned: evidence from Jurassic and Proterozoic ^{40}Ar/^{39}Ar ages and geochemistry of the giant Okavango dike swarm (Botswana). Earth Planet. Sci. Lett. 222, 989-1006. http://dx.doi.org/10.1016/j.epsl.2004.03.017.

Jourdan, F., Féraud, G., Bertrand, H., Kampunzu, A.B., Tshoso, G., Watkeys, M.K., Le Gall, B., 2005. Karoo large igneous province: Brevity, origin, and relation to mass extinction questioned by new ^{40}Ar/^{39}Ar age data. Geology 33, 745-748. http://dx.doi.org/10.1130/G21632.1.

Jourdan, F., Féraud, G., Bertrand, H., Watkeys, M.K., Kampunzu, A.B., Le Gall, B., 2006. Basement control on dyke distribution in large igneous provinces: case study of the Karoo triple junction. Earth Planet. Sci. Lett. 241, 307-322. http://dx.doi.org/10.1016/j.epsl.2005.10.003.

Jourdan, F., Bertrand, H., Schaerer, U., Blichert-Toft, J., Féraud, G., Kampunzu, A.B., 2007a. Major and trace element and Sr, Nd, Hf, and Pb isotope compositions of the Karoo large igneous province, Botswana-Zimbabwe: lithosphere vs mantle plume contribution. J. Petrol. 48, 1043-1077. http://dx.doi.org/10.1093/petrology/egm010.

Jourdan, F., Féraud, G., Bertrand, H., Watkeys, M.K., 2007b. From flood basalts to the inception of oceanization: example from the ^{40}Ar/^{39}Ar high-resolution picture of the Karoo large igneous province. Geochem. Geophys. Geosyst. 8. http://dx.doi.org/10.1029/2006GC001392.

Jourdan, F., Bertrand, H., Feraud, G., Le Gall, B., Watkeys, M.K., 2009. Lithospheric mantle evolution monitored by overlapping large igneous provinces: case study in southern Africa. Lithos 107, 257-268. http://dx.doi.org/10.1016/j.lithos.2008.10.011.

Kent, A.J.R., Stolper, E.M., Francis, D., Woodhead, J., Frei, R., Eiler, J., 2004. Mantle heterogeneity during the formation of the North Atlantic Igneous Province: Constraints from trace element and Sr-Nd-Os-O isotope systematics of Baffin Island picrites. Geochem. Geophys. Geosyst. 5. http://dx.doi.org/10.1029/2004GC000743.

Kerr, A.C., Saunders, A.D., Tarney, J., Berry, N.H., Hards, V.L., 1995. Depleted mantle-plume geochemical signatures: No paradox for plume theories. Geology 23, 843-846. http://dx.doi.org/10.1130/0091-7613(1995)023<0843:dmpgsn>2.3.co;2.

Krogh, T.E., 1982. Improved accuracy of U-Pb zircon ages by the creation of more concordant systems using an air abrasion technique. Geochim. Cosmochim. Acta 46, 637-649. http://dx.doi.org/10.1016/0016-7037(82)90165-X.

Kurz, M.D., 1986. Cosmogenic helium in a terrestrial igneous rock. Nature 320, 435-439. http://dx.doi.org/10.1038/320435a0.

Kurz, M.D., Jenkins, W.J., 1981. The distribution of helium in oceanic basalt glasses. Earth Planet. Sci. Lett. 53, 41-54. http://dx.doi.org/10.1016/0012-821X(81)90024-8.

Kurz, M.D., Jenkins, W.J., Hart, S.R., 1982. Helium isotopic systematics of oceanic islands and mantle heterogeneity. Nature 297, 43-47. http://dx.doi.org/10.1038/297043a0.

Kurz, M.D., Kenna, T.C., Lassiter, J.C., DePaolo, D.J., 1996. Helium isotopic evolution of Mauna Kea Volcano: First results from the 1-km drill core. J. Geophys. Res. B 101, 11781-11791. http://dx.doi.org/10.1029/95JB03345.

Kurz, M.D., Curtice, J., Lott, D.E., Solow, A., 2004. Rapid helium isotopic variability in Mauna Kea shield lavas from the Hawaiian Scientific Drilling Project. Geochem. Geophys. Geosyst. 5. http://dx.doi.org/10.1029/2002GC000439.

Langmuir, C.H., Klein, E.M., Plank, T., 1992. Petrological Systematics of Mid-Ocean Ridge Basalts: Constraints on Melt Generation Beneath Ocean Ridges. In: Morgan, J.P., Blackman, D.K., Sinton, J.M. (Eds.), Mantle Flow and Melt Generation at Mid-Ocean Ridges. Geoph. Monog. Series 71, AGU, pp. 183-280. http://dx.doi.org/10.1029/gm071p0183.

Le Gall, B., Tshoso, G., Jourdan, F., Féraud, G., Bertrand, H., Tiercelin, J.J., Kampunzu, A.B., Modisi, M.P., Dyment, J., Maia, M., 2002. ^{40}Ar/^{39}Ar geochronology and structural data from the giant Okavango and related mafic dyke swarms, Karoo igneous province, northern Botswana. Earth Planet. Sci. Lett. 202, 595-606. http://dx.doi.org/10.1016/s0012-821x(02)00763-x.

Le Gall, B., Tshoso, G., Dyment, J., Basira Kampunzu, A., Jourdan, F., Féraud, G., Bertrand, H., Aubourg, C., Vétel, W., 2005. The Okavango giant mafic dyke swarm (NE Botswana): its structural significance within the Karoo Large Igneous Province. J. Struct. Geol. 27, 2234-2255. http://dx.doi.org/10.1016/j.jsg.2005.07.004.

le Roex, A.P., Dick, H.J.B., Fisher, R.L., 1989. Petrology and geochemistry of MORB from 25°E to 46°E along the Southwest Indian Ridge: evidence for contrasting styles of mantle enrichment. J. Petrol. 30, 947-986. http://dx.doi.org/10.1093/petrology/30.4.947.

Le Roux, V., Dasgupta, R., Lee, C.-A., 2011. Mineralogical heterogeneities in the Earth's mantle: Constraints from Mn, Co, Ni and Zn partitioning during partial melting. Earth Planet. Sci. Lett. 307, 395-408. http://dx.doi.org/10.1016/j.epsl.2011.05.014.

Lightfoot, P.C., Hawkesworth, C.J., Olshefsky, K., Green, T., Doherty, W., Keays, R.R., 1997. Geochemistry of Tertiary tholeiites and picrites from Qeqertarssuaq (Disko Island) and Nuussuaq, West Greenland with implications for the mineral potential of comagmatic intrusions. Contrib. Mineral. Petrol. 128, 139-163. http://dx.doi.org/10.1007/s004100050300.

Lintinen, P., Nenonen, J., 1997. Glacial history of the Vestfjella and Heimefrontfjella nunatak ranges in western Dronning Maud Land, Antarctica. In: Ricci, C.A. (Ed.), The Antarctic Region: Geological Evolution and Processes. Siena: Terra Antarctica Publications, Italy, pp. 845-852.

Liu, X., Huang, F., Kong, P., Fang, A., Li, X., Ju, Y., 2010. History of ice sheet elevation in East Antarctica: Paleoclimatic implications. Earth Planet. Sci. Lett. 290, 281-288. http://dx.doi.org/10.1016/j.epsl.2009.12.008.

Lupton, J.E., Craig, H., 1975. Excess ^{3}He in oceanic basalts: Evidence for terrestrial primordial helium. Earth Planet. Sci. Lett. 26, 133-139. http://dx.doi.org/10.1016/0012-821X(75)90080-1.

Luttinen, A.V., Furnes, H., 2000. Flood basalts of Vestfjella: Jurassic magmatism across an Archaean-Proterozoic lithospheric boundary in Dronning Maud Land, Antarctica. J. Petrol. 41, 1271-1305. http://dx.doi.org/10.1093/petrology/41.8.1271.

Luttinen, A.V., Heinonen, J.S., Kurhila, M., Jourdan, F., Mänttäri, I., Vuori, S., Huhma, H., 2015. Depleted mantle-sourced CFB magmatism in the Jurassic Africa-Antarctica rift: petrology and ^{40}Ar/^{39}Ar and U/Pb chronology of the Vestfjella dyke swarm, Dronning Maud Land, Antarctica. J. Petrol. 56, 919-952. http://dx.doi.org/10.1093/petrology/egv022.

Mahoney, J.J., Natland, J.H., White, W.M., Poreda, R., Bloomer, S.H., Fisher, R.L., Baxter, A.N., 1989. Isotopic and geochemical provinces of the western Indian Ocean Spreading Centers. J. Geophys. Res. B 94, 4033-4052, http://dx.doi.org/10.1029/JB094iB04p04033.

Mahoney, J.J., le Roex, A.P., Peng, Z., Fisher, R.L., Natland, J.H., 1992. Southwestern limits of Indian Ocean ridge mantle and the origin of low ^{206}Pb/^{204}Pb mid-ocean ridge basalt: isotope systematics of the central Southwest Indian Ridge (17°-50°E). J. Geophys. Res. B 97, 19771-19790. http://dx.doi.org/10.1029/92JB01424.

Melluso, L., Morra, V., Brotzu, P., Mahoney, J.J., 2001. The Cretaceous Igneous Province of Madagascar: Geochemistry and Petrogenesis of Lavas and Dykes from the Central–Western Sector. J. Petrol. 42, 1249-1278. http://dx.doi.org/10.1093/petrology/42.7.1249.

Melluso, L., Morra, V., Brotzu, P., Tommasini, S., Renna, M.R., Duncan, R.A., Franciosi, L., D'Amelio, F., 2005. Geochronology and Petrogenesis of the Cretaceous Antampombato–Ambatovy Complex and Associated Dyke Swarm, Madagascar. J. of Petrol. 46, 1963-1996. http://dx.doi.org/10.1093/petrology/egi044.

Molzahn, M., Reisberg, L., Wörner, G., 1996. Os, Sr, Nd, Pb, O isotope and trace element data from the Ferrar flood basalts, Antarctica: evidence for an enriched subcontinental lithospheric source. Earth Planet. Sci. Lett. 144, 529-545. http://dx.doi.org/10.1016/S0012-821X(96)00178-1.

Nicolaysen, K.P., Frey, F.A., Mahoney, J.J., Johnson, K.T.M., Graham, D.W., 2007. Influence of the Amsterdam/St. Paul hot spot along the Southeast Indian Ridge between 77° and 88°E: Correlations of Sr, Nd, Pb, and He isotopic variations with ridge segmentation. Geochem. Geophys. Geosyst. 8. http://dx.doi.org/10.1029/2006GC001540.

Neumann, E., Svensen, H., Galerne, C.Y., Planke, S., 2011. Multistage Evolution of Dolerites in the Karoo Large Igneous Province, Central South Africa. J. Petrol. 52, 959-984. http://dx.doi.org/10.1093/petrology/egr011.

Porcelli, D., Ballentine, C.J., 2002. Models for Distribution of Terrestrial Noble Gases and Evolution of the Atmosphere. In: Porcelli, D., Ballentine, C.J., Wieler, R. (Eds.), Noble Gases in Geochemistry and Cosmochemistry. Rev. Mineral. Geochem. 47, Min. Soc. Am., Washington DC, United States, pp. 411-480. http://dx.doi.org/10.2138/rmg.2002.47.11.

Putirka, K.D., Perfit, M., Ryerson, F.J., Jackson, M.G., 2007. Ambient and excess mantle temperatures, olivine thermometry, and active vs. passive upwelling. Chem. Geol. 241, 177-206. http://dx.doi.org/10.1016/j.chemgeo.2007.01.014.

Richards, M.A., Duncan, R.A., Courtillot, V.E., 1989. Flood basalts and hot-spot tracks: plume heads and tails. Science 246, 103-107. http://dx.doi.org/10.1126/science.246.4926.103.

Riley, T.R., Leat, P.T., Curtis, M.L., Millar, I.L., Duncan, R.A., Fazel, A., 2005. Early-Middle Jurassic dolerite dykes from Western Dronning Maud Land (Antarctica): Identifying mantle sources in the Karoo Large Igneous Province. J. Petrol. 46, 1489-1524. http://dx.doi.org/10.1093/petrology/egi023.

Rolf, T., Coltice, N., Tackley, P.J., 2012. Linking continental drift, plate tectonics and the thermal state of the Earth's mantle. Earth Planet. Sci. Lett. 351–352, 134-146. http://dx.doi.org/10.1016/j.epsl.2012.07.011.

Ryan, J.G., Langmuir, C.H., 1993. The systematics of boron abundances in young volcanic rocks. Geochim. Cosmochim. Acta 57, 1489-1498. http://dx.doi.org/10.1016/0016-7037(93)90008-K.

Salters, V.J.M., Stracke, A., 2004. Composition of the depleted mantle. Geochem. Geophys. Geosyst. 5. http://dx.doi.org/10.1029/2003gc000597.

Sarda, P., Moreira, M., Staudacher, T., Schilling, J., Allègre, C.J., 2000. Rare gas systematics on the southernmost Mid-Atlantic Ridge: Constraints on the lower mantle and the Dupal source. J. Geophys. Res. B 105, 5973-5996. http://dx.doi.org/10.1029/1999JB900282.

Silver, P.G., Behn, M.D., Kelley, K.A., Schmitz, M., Savage, B., 2006. Understanding cratonic flood basalts. Earth Planet. Sci. Lett. 245, 190-201. http://dx.doi.org/10.1016/j.epsl.2006.01.050.

Starkey, N.A., Stuart, F.M., Ellam, R.M., Fitton, J.G., Basu, S., Larsen, L.M., 2009. Helium isotopes in early Iceland plume picrites: Constraints on the composition of high ^{3}He/^{4}He mantle. Earth Planet. Sci. Lett. 277, 91-100. http://dx.doi.org/10.1016/j.epsl.2008.10.007.

Stone, J.O., 2000. Air pressure and cosmogenic isotope production. J. Geophys. Res. B 105, 23753-23759. http://dx.doi.org/10.1029/2000JB900181.

Storey, M., Mahoney, J.J., Saunders, A.D., 1997. Cretaceous basalts in Madagascar and the transition between plume and continental lithosphere mantle sources. In: Mahoney, J.J., Coffin, M.F. (Eds.), Large igneous provinces: continental, oceanic, and planetary flood volcanism. Geoph. Monog. Series 71, AGU, pp. 95-122. http://dx.doi.org/10.1029/gm100p0095.

Stroncik, N.A., Haase, K.M., 2004. Chlorine in oceanic intraplate basalts: Constraints on mantle sources and recycling processes. Geology 32, 945-948. http://dx.doi.org/10.1130/G21027.1.

Stuart, F.M., Lass-Evans, S., Godfrey Fitton, J., Ellam, R.M., 2003. High ^{3}He/^{4}He ratios in picritic basalts from Baffin Island and the role of a mixed reservoir in mantle plumes. Nature 424, 57-59. http://dx.doi.org/10.1038/nature01711.

Sweeney, R.J., Duncan, A.R., Erlank, A.J., 1994. Geochemistry and petrogenesis of central Lebombo basalts of the Karoo igneous province. J. Petrol. 35, 95-125. http://dx.doi.org/10.1093/petrology/35.1.95.

Thompson, R.N., Gibson, S.A., Dickin, A.P., Smith, P.M., 2001. Early Cretaceous basalt and picrite dykes of the southern Etendeka region, NW Namibia: Windows into the role of the Tristan mantle plume in Parana-Etendeka magmatism. J. Petrol. 42, 2049-2081. http://dx.doi.org/10.1093/petrology/42.11.2049

Watkeys, M.K., 2002. Development of the Lebombo rifted volcanic margin of Southeast Africa. In: Menzies, M.A., Klemperer, S.L., Ebinger, C.J., Baker, J. (Eds.), Volcanic rifted margins. Geol. Soc. Am. Spec. Paper 362, Boulder CO, United States, pp. 27-46. http://dx.doi.org/10.1130/0-8137-2362-0.27.

Workman, R.K., Hart, S.R., 2005. Major and trace element composition of the depleted MORB mantle (DMM). Earth Planet. Sci. Lett. 231, 53-72. http://dx.doi.org/10.1016/j.epsl.2004.12.005.